The Substrate-Bound Type 2 Copper Site of Nitrite Reductase: The Nitrogen Hyperfine Coupling of Nitrite Revealed by Pulsed EPR†

Maria Fittipaldi,‡ Hein J. Wijma,§ Martin P. Verbeet,§ Gerard W. Canters,§ Edgar J. J. Groenen,‡ and Martina Huber*,‡

Department of Molecular Physics, Huygens Laboratory, Leiden University, P.O. Box 9504, and Gorlaeus Laboratories, Metallo Protein Group, Leiden University, P.O. Box 9502, 2300 RA Leiden, The Netherlands

Received July 17, 2005; Revised Manuscript Received September 27, 2005

ABSTRACT: A pulsed electron paramagnetic resonance study has been performed on the type 2 copper site of nitrite reductase (NiR) from *Alcaligenes faecalis*. The H145A mutant, in which histidine 145 is replaced by alanine, was studied by ESEEM and HYSCORE experiments at 9 GHz on frozen solutions. This mutant contains a reduced type 1 copper site which allowed a selective investigation of the type 2 site of H145A and of its nitrite-bound form H145A (NO_2^-). The experiments yielded hyperfine and quadrupole parameters of the remote nitrogens of two of the histidines in the type 2 copper site of the protein and revealed the changes of these values induced by substrate binding ($^{14}NO_2^-$ and $^{15}NO_2^-$). The HYSCORE experiments displayed a signal of $^{15}NO_2^-$ bound to H145A, from which hyperfine parameters of the nitrite nitrogen were estimated. The small isotropic hyperfine coupling, 0.36 MHz, of the nitrite nitrogen (^{14}N) suggests that the substrate binds in an axial position to the copper in the type 2 site and that the molecular orbital containing the unpaired electron extends onto the substrate. This and other changes in the EPR parameters occurring after nitrite binding suggest a change in electronic structure of the site, which most likely prepares the site for the catalytic reaction. We propose that this change is essential for the reaction to occur.

The global nitrogen cycle is governed in part by life-dependent processes, one of which deals with the denitrification of soil and aqueous systems. Bacterial denitrification is mediated by copper- and heme-containing enzymes, such as the copper-containing nitrite reductase (NiR)[1] (*1*). NiR catalyzes the reduction of nitrite to nitric oxide according to the overall reaction:

$$NO_2^- + 2H^+ + e^- \rightarrow NO + H_2O$$

The X-ray structure revealed that these nitrite reductases (*2*, *3*) are homotrimers and contain two distinct copper sites per monomer: a type 1 and a type 2 site (Figure 1). The type 1 copper site has the typical coordination of blue copper proteins (two nitrogens deriving from two histidine residues, a sulfur of a cysteine, and a weaker axial sulfur ligand from a methionine). At the type 2 site, copper is coordinated by three histidine nitrogens and a water molecule. The two copper sites are directly linked by a Cys−His bridge (see Figure 1). The distance between the copper ions is about 12.5 Å. The type 1 site of NiR functions as an electron transfer site (*4*). The type 2 copper site is the catalytic site where nitrite binds and is reduced. The binding geometry was characterized in detail by structural studies (*5*, *6*), which showed that the nitrite binds via the oxygen atoms. In these studies the substrate was suggested to bind to the oxidized type 2 copper site. According to this result and other

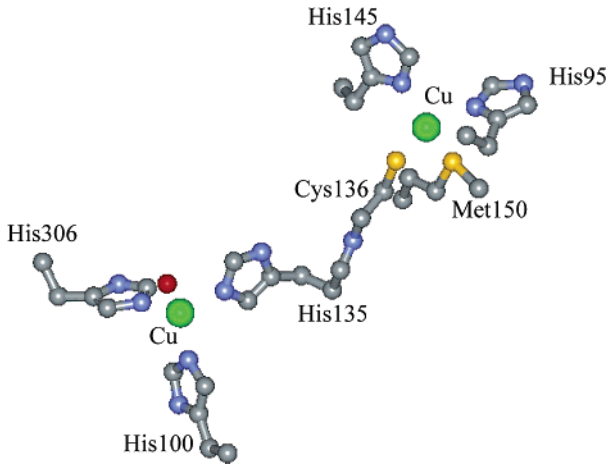

FIGURE 1: Ligation of the two copper ions in the active site of nitrite reductase. The copper in the type 1 site (upper part of the figure) is bound to the two N_δ's of His95 and His145, the S_δ of Met150, and the S_γ of Cys136. The copper in the type 2 site (lower part of the figure) is bound to the three N_ϵ's of His135, His100, and His306. The oxygen of the water molecule bound to the type 2 site is shown.

† This work was performed under the auspices of the BIOMAC research school of Leiden University.

* To whom correspondence should be addressed. Phone: +31 71 527 5560. Fax: +31 71 527 5819. E-mail: mhuber@molphys.leidenuniv.nl.

‡ Department of Molecular Physics, Huygens Laboratory, Leiden University.

§ Gorlaeus Laboratories, Metallo Protein Group, Leiden University.

[1] Abbreviations: NiR, nitrite reductase; EPR, electron paramagnetic resonance; ESEEM, electron spin−echo envelope modulation; HYSCORE, hyperfine sublevel correlation; ENDOR, electron nuclear double resonance; H145A, mutant of NiR; SOMO, singly occupied molecular orbital.

10.1021/bi0513913 CCC: $30.25
Published on Web 10/29/2005

investigations (*7*−*9*), substrate binding precedes electron transfer from the type 1 to the type 2 site, although recent evidence points in the direction of a random sequential mechanism (H. J. Wijma, unpublished results). The nitrite is converted at the type 2 copper site into nitric oxide (NO), and an NO-bound form of the enzyme has been characterized by crystallography (*6*).

EPR studies revealed changes in the electronic structure of the type 2 copper site upon nitrite binding, such as a change in the copper hyperfine interaction (A_{zz}) and an increased rhombicity of the *g*-tensor (*10*). No interpretation of these changes with respect to the mechanism was given. An electron nuclear double resonance (ENDOR) study at X-band (9 GHz) of NiR (*11*) and ENDOR studies at Q-band (34 GHz) of NiR and mutants thereof (*12*, *13*) revealed changes in the hyperfine coupling of the coordinating nitrogens of the type 2 copper site upon binding of nitrite but did not reveal any nitrite signal. The absence of a nitrogen signal of nitrite was ascribed to the binding of nitrite in an axial position from which a weak coupling is expected.

We performed electron spin−echo envelope modulation (ESEEM) and hyperfine sublevel correlation (HYSCORE) experiments at X-band on the H145A mutant of NiR from *Alcaligenes faecalis* and its nitrite-bound complex. In this mutant, where histidine 145 is replaced by alanine, the midpoint potential of the copper in the type 1 site has increased by several hundreds of millivolts, and it is easy, therefore, to keep the site reduced (*14*) and, thus, EPR silent. This situation is ideal for the EPR investigation of the type 2 site of NiR where nitrite binds. The aim of the present study was to look for the nitrogen of the substrate nitrite bound to the type 2 copper site. At the X-band, deep modulations in the ESEEM spectra are expected for weakly coupled nitrogens, with an isotropic hyperfine coupling of the order of 1−2 MHz, thus increasing the chances to detect a weakly coupled nitrite nitrogen. The two-dimensional HYSCORE experiment has intrinsically a higher resolution and simplifies the interpretation of ESEEM spectra by allowing detection of the correlation of the nuclear sublevels of the two electron spin manifolds. The search for the hyperfine coupling of the nitrite nitrogen is motivated by the fact that it is the most direct way to determine the delocalization of the singly occupied molecular orbital (SOMO) onto the substrate. Combining this result with the other changes of the EPR parameters of the type 2 site upon substrate binding enabled us to propose a model for the electronic changes of the site upon nitrite binding in relation to the reaction mechanism.

MATERIALS AND METHODS

The construction of the H145A mutant, protein preparation, and purification have been described elsewhere (*14*). The Cu content was 2.0 per monomer, indicating full occupation of the type 1 and type 2 sites.

The solutions used for the EPR experiments had a concentration of approximately 0.7 mM protein with 30% glycerol and 35 mM MES at pH 6.0. For the solutions with nitrite bound to H145A approximately 6 mM $NaNO_2$ was added.

All measurements, cw EPR, ESEEM, and HYSCORE, on frozen solutions were performed using a 9 GHz ELEXSYS E 680 spectrometer (Bruker, Rheinstetten, Germany). The cw EPR spectra were acquired at 40 K. The amplitude and frequency of the modulation were respectively 0.5 mT and 100 kHz. The spectra were recorded using a microwave power of 0.6 mW, and the total measurement time was 21 min per spectrum.

The ESEEM and HYSCORE experiments were performed at 10 K. The ESEEM data were acquired using the pulse sequence $\pi/2-\tau-\pi/2-T-\pi/2-\tau-$echo. To compensate for blind spots, spectra were measured using τ values of 140, 188, and 212 ns. The following parameters were used: length of the $\pi/2$ pulse, $t_{\pi/2} = 16$ ns; starting time, $T = 200$ ns; time increments, $\Delta t = 16$ ns; and number of points used, 1500. A four-step phase cycle was used to remove artifacts from unwanted echoes (*15*). For each step of the phase cycle the number of time traces accumulated was one for the ESEEM experiment at the intermediate magnetic field value of the EPR spectrum (cf. Figure 2) and four for the low- and high-field values. For both ESEEM and HYSCORE measurements, a shot repetition time of 3.2 ms and 20 shots per loop were used.

Data processing was done using the Xepr program (Bruker, Rheinstetten, Germany). The ESEEM time traces were baseline corrected using an exponential decay function, apodized with a Hamming window, and zero filled. After the Fourier transformation of the real and imaginary part, the absolute value was calculated.

The HYSCORE spectra were recorded using the pulse sequence $\pi/2-\tau-\pi/2-t_1-\pi-t_2-\pi/2-\tau-$echo. A four-step phase cycle was used to remove artifacts from unwanted echoes (*15*). To realize the pulse sequence, four different pulse channels were utilized. The following parameters were used: length of the pulses, $t_{\pi/2} = 32$ ns and $t_\pi = 28$ ns; $\tau = 144$ ns; starting time, $t_1 = 56$ ns and $t_2 = 200$ ns; and time increments, $\Delta t = 24$ ns (data matrix 256 × 256). Two different pulse channels provided the $\pi/2$ and π pulses. This allowed an independent variation of the microwave power level and of the excitation bandwidth. For each step of the phase cycle one sweep was used. The total measurement time was about 5 h. A bandwidth filter setting of 50 MHz was employed.

Data processing was done using the Xepr program (Bruker, Rheinstetten, Germany). The HYSCORE time traces were baseline corrected using a linear fit for both the real and imaginary part, apodized with a Hamming window, and zero filled. After the Fourier transformation, the absolute values were calculated in order to obtain contour plots.

The cw EPR spectra were simulated using the Bruker program SYMFONIA. The ESEEM spectra were simulated according to the procedure described elsewhere (*16*). Simulations of the HYSCORE spectra were performed using an extension of the program for the ESEEM simulations (*17*).

RESULTS

Figure 2 shows the 9 GHz cw EPR spectra of frozen solutions of NiR and of H145A without and with nitrite bound. As indicated in Figure 2A, the EPR spectrum of NiR is a superposition of the EPR signals of the type 1 and type 2 copper sites. The EPR signal of H145A (Figure 2B) derives

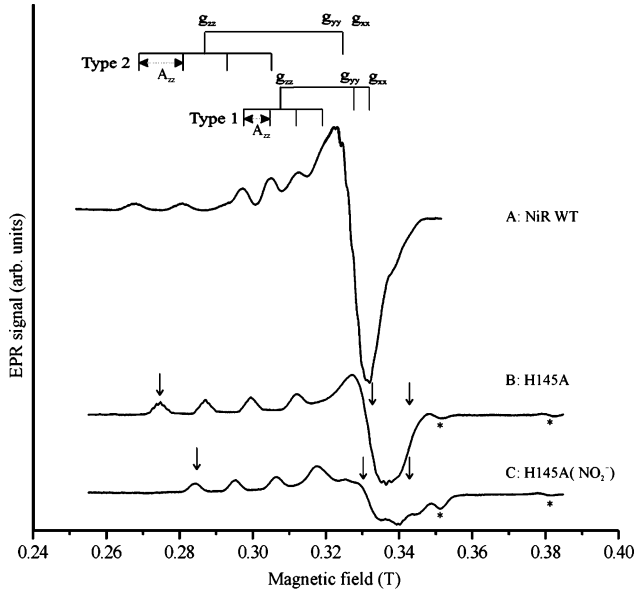

FIGURE 2: cw EPR spectra of frozen solutions of (A) NiR, (B) H145A, and (C) H145A (NO_2^-). The spectra have been acquired at different microwave frequencies: 9.48 GHz (A), 9.73 GHz (B), and 9.74 GHz (C). The features marked with an asterisk in (B) and (C) are artifacts of the spectrometer. The arrows indicate the magnetic field values at which the ESEEM spectra have been acquired.

Table 1: *g* Values and Copper Hyperfine Parameters of the Type 1 and Type 2 Copper Sites of wt NiR and the H145A Mutant

enzyme	copper site	g_{zz}	g_{yy}	g_{xx}	A_{zz} (mT)
wt NiR	type 1	2.1951[a]	2.055[a]	2.025[a]	7.5
	type 2	2.358	2.076[a]	2.076[a]	13.0
H145A	type 2	2.368	2.088	2.081	12.6
H145A (NO_2^-)	type 2	2.315	2.130	2.045	10.9

[a] Values obtained from cw EPR measurements at 95 GHz (Fittipaldi et al., manuscript in preparation); remaining parameters from simulation of the 9 GHz EPR spectra.

from the type 2 copper site. Comparison between parts A and B of Figure 2 reveals small differences in the g_{zz} and A_{zz} values of the type 2 copper sites (see Table 1). Figure 2C shows the EPR spectrum of H145A with nitrite bound. The EPR parameters, principal *g* values and copper A_{zz} value, of H145A change upon nitrite binding. The simulations of the EPR spectra yield the *g* values and the copper hyperfine parameters of the different enzymes (cf. Table 1). In particular, a decrease of the g_{zz} and A_{zz} values and an increase of the rhombicity of the *g*-tensor are observed upon binding of nitrite to H145A (see Table 1).

In Figure 3, the X-band ESEEM spectra of frozen solutions of H145A (upper traces) and of H145A (NO_2^-), with $^{14}NO_2^-$ (middle traces) and $^{15}NO_2^-$ (lower traces), are shown. The ESEEM spectra were acquired at three magnetic field values corresponding to different orientations of the magnetic field with respect to the *g* axes. Spectra acquired at τ values of 140 and 188 ns are shown. The ESEEM spectra of H145A are characterized by several intense bands below about 1.7 MHz and by broad bands between 2.5 and 4.5 MHz. The bands below 1.7 MHz show little orientation dependence of the frequencies, while their relative intensities change considerably upon changing the orientation and τ.

Comparison of the ESEEM spectra (Figure 3) of H145A with and without nitrite bound reveals an overall change in the ESEEM pattern of H145A upon binding of nitrite. A shift of the broad band around 3.5 MHz toward lower frequencies, a broadening of the bands, and a decrease in intensity of the bands around 0.6−0.8 MHz are observed as a result of nitrite binding. Much smaller differences are observed between the ESEEM spectra of H145A (NO_2^-) with $^{14}NO_2^-$ and $^{15}NO_2^-$. When $^{14}NO_2^-$ is replaced by $^{15}NO_2^-$, the ESEEM spectra remain largely unchanged except for the marked feature in Figure 3B,E.

In Figure 4, the HYSCORE spectra of H145A (Figure 4A) and of H145A (NO_2^-), with $^{14}NO_2^-$ (Figure 4B) and $^{15}NO_2^-$ (Figure 4C), are shown. In the HYSCORE spectrum of H145A, prominent features are ridges in the ++ quadrant at (3.87, 1.54) and (3.80, 0.80) MHz, labeled d and e, and ridges in the −+ quadrant at (−4.19, 1.46), (−4.20, 0.83), and (−3.87, 1.54) MHz, labeled a, b, and d1, which run parallel to the ν_2 frequency axis. Prominent diagonal peaks occur in the ++ quadrant around (1.5, 1.5), (0.8, 0.8), and (0.6, 0.6) MHz. In the HYSCORE spectra of H145A (NO_2^-) (Figure 4B,C), ridges running parallel to the ν_2 frequency axis are present around (3.57, 0.88) and (3.74, 1.55) MHz, labeled e and d, respectively. The HYSCORE spectra differ from that of H145A, in that the frequencies ν_2 of the ridges decrease, while the ridges corresponding to a and d1 in H145A can no longer be distinguished. Compared to H145A ($^{14}NO_2^-$), the HYSCORE spectrum of H145A ($^{15}NO_2^-$) shows an additional ridge (labeled f in Figure 4C), which runs almost perpendicular to the diagonal starting from approximately (1.5, 1.5) MHz.

Data Analysis. The nuclear spin Hamiltonian of each nucleus coupled to the unpaired electron spin ($S = {}^1/_2$) consists of the nuclear Zeeman interaction, the hyperfine interaction, and, for nuclei with $I = 1$, the quadrupole interaction:

$$H_n = -g_n\beta_N\vec{I}_n\vec{B}_0 + \langle\vec{S}\rangle_{\alpha,\beta}\underline{A}_n\vec{I}_n + \vec{I}_n\underline{Q}_n\vec{I}_n \qquad (1)$$

where g_n is the nuclear *g*-factor, β_N the nuclear Bohr magneton, $\vec{B}_0$ the external magnetic field, $\vec{I}_n$ the nuclear spin angular momentum operator, $\langle\vec{S}\rangle$ the expectation value of the electron spin angular momentum operator in the two electron spin manifolds, $\underline{A}_n$ and $\underline{Q}_n$ the hyperfine and quadrupole tensors, respectively.

For a nuclear spin $I = 1$, for each of the two electron spin manifolds (α, β), three transitions between the nuclear sublevels are possible, two single-quantum (sq) transitions with $|\Delta M_I| = 1$ and one double-quantum (dq) transition with $|\Delta M_I| = 2$.

In the so-called cancellation condition, $|A_{iso}| \approx 2\nu_I$, the isotropic hyperfine interaction (A_{iso}) about cancels the nuclear Zeeman interaction in the α electron spin manifold (assuming A_{iso} positive). As a consequence, the ESEEM frequencies within this manifold are approximately the nuclear quadrupole (NQ) frequencies, ν_0, ν_-, and ν_+. These frequencies obey the relation

$$\nu_0 + \nu_- = \nu_+ \qquad (2)$$

The quadrupole parameters of the nucleus $|e^2qQ/h| = 4K$

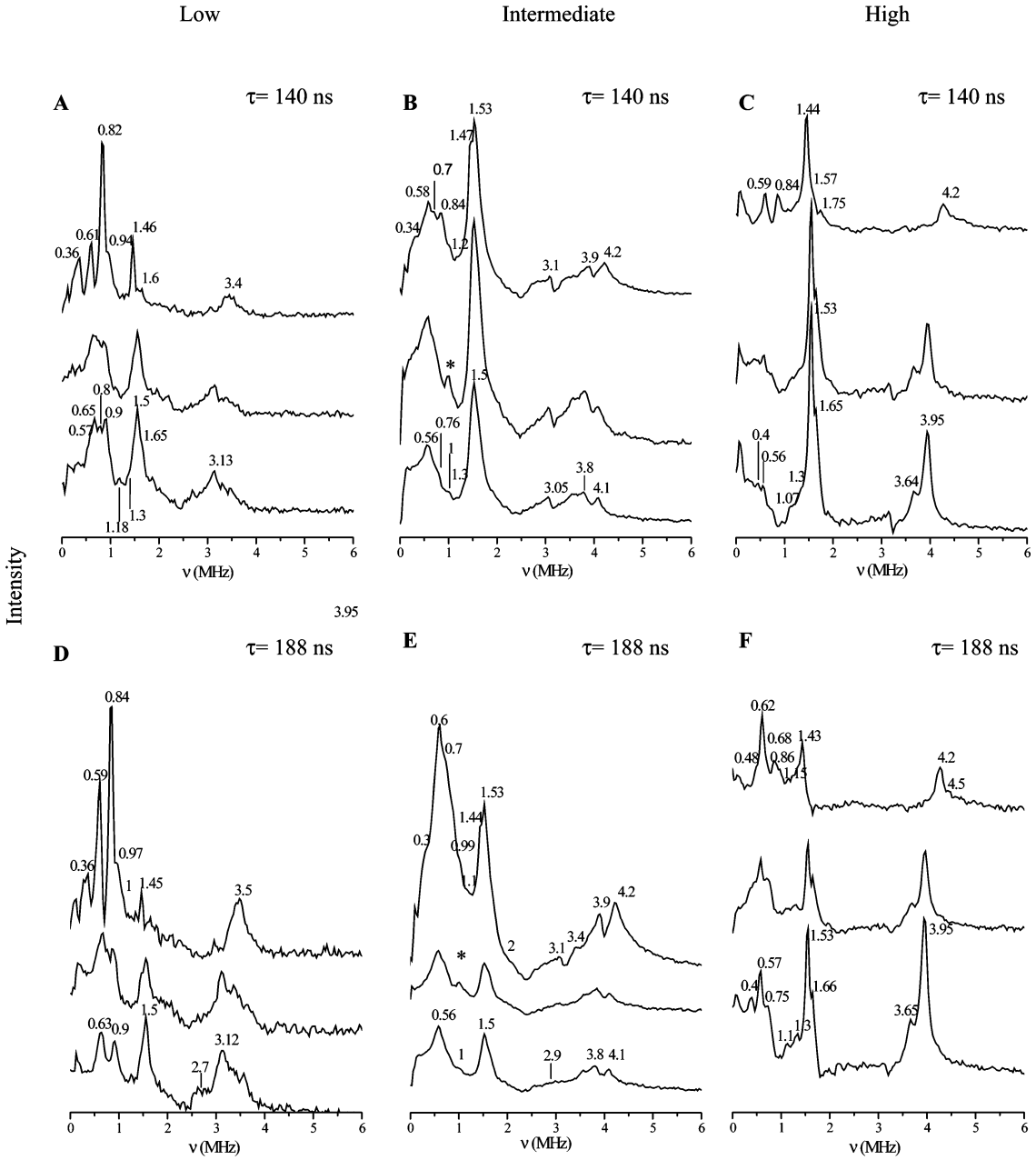

FIGURE 3: ESEEM spectra of frozen solutions of H145A, H145A ($^{14}NO_2^-$), and H145A ($^{15}NO_2^-$) (upper trace, middle trace, and lower trace in each panel, respectively). The ESEEM spectra in (A), (B), and (C) have been acquired at low, intermediate, and high magnetic field values as indicated by the arrows in the EPR spectra of Figure 2 and using a τ value of 140 ns. The ESEEM spectra in (D), (E), and (F) have been acquired at the same low, intermediate, and high magnetic field values and using a τ value of 188 ns.

and η are given by

$$\nu_0 = 2K\eta$$

$$\nu_- = K(3 - \eta)$$

$$\nu_+ = K(3 + \eta) \qquad (3)$$

At these frequencies in the ESEEM spectra narrow lines appear, the position of which is approximately orientation-independent. In the other electron spin manifold (β), the hyperfine and the Zeeman interaction add and three transitions exist, two single-quantum transitions ($\nu_{sq}\beta$) and one double-quantum transition ($\nu_{dq}\beta$). The lines at $\nu_{sq}\beta$'s are generally not visible in the ESEEM spectra of powders due to the large inhomogeneous broadening. From the frequency of the double-quantum transition, the value of A_{iso} can be obtained from

$$|A_{iso}| = \frac{\nu_{dq\beta}^2 - \nu_+^2}{8\nu_I} \qquad (4)$$

provided that the anisotropic hyperfine coupling is small compared to A_{iso} (*18*).

The remote nitrogens of the histidines coordinated to copper centers have $|A_{iso}|$ values of 1−2 MHz (*19*, *20*). They meet the cancellation condition at about 9 GHz. For these nitrogens, $\nu_{dq\beta}$ appears in the ESEEM spectra as a broad feature around 4 MHz.

The HYSCORE spectra contain cross-peaks which allow to correlate nuclear frequencies of the α and β manifolds.

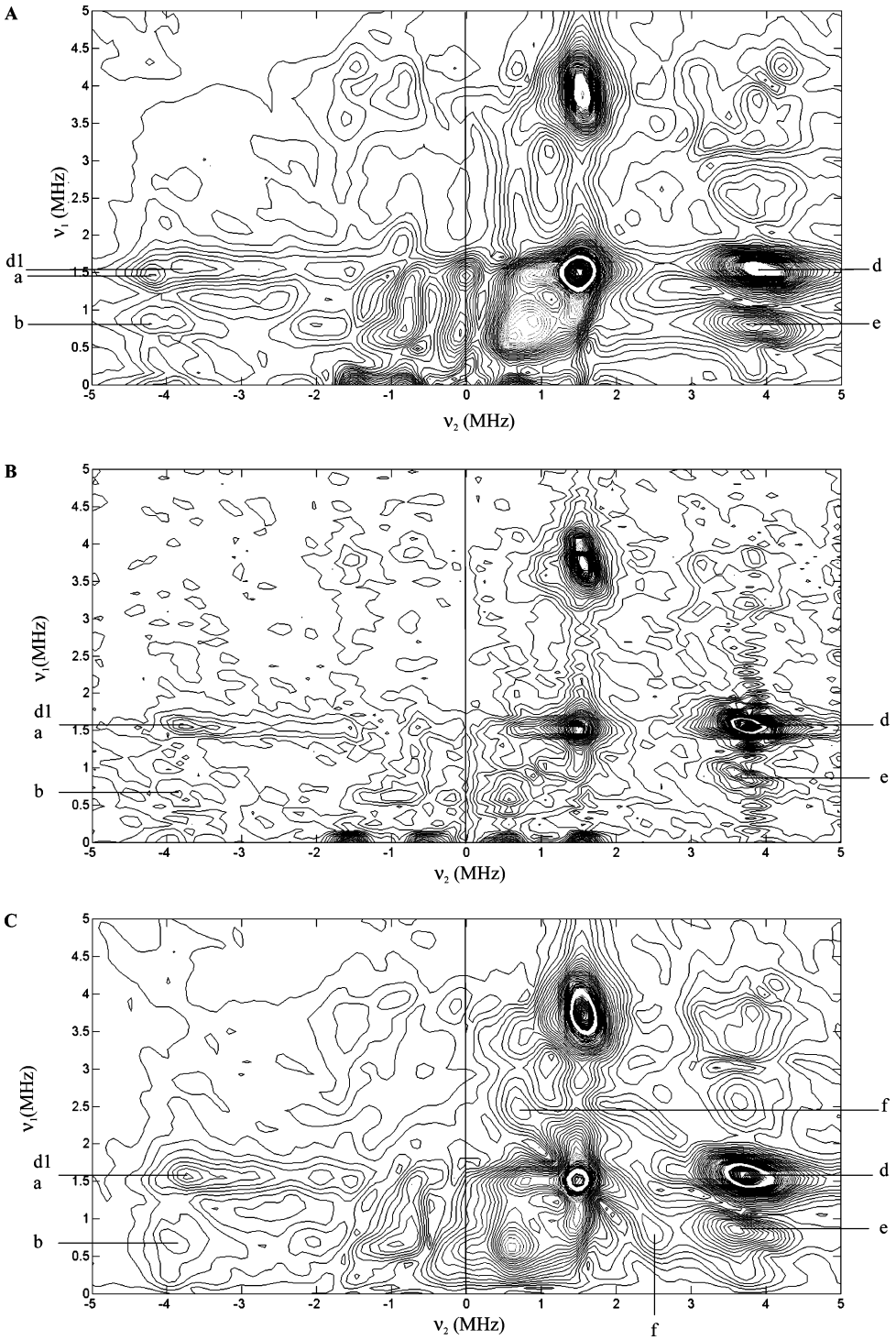

FIGURE 4: HYSCORE contour plots for frozen solutions of (A) H145A, (B) H145A ($^{14}NO_2^-$), and (C) H145A ($^{15}NO_2^-$), acquired at the respective intermediate magnetic field values using $\tau = 144$ ns. To facilitate comparison, contour levels of the three HYSCORE spectra were calculated at the same values.

For remote nitrogens, three peaks are expected, those correlating ν_0, ν_-, and ν_+ with $\nu_{dq\beta}$. Moreover, for nitrogens close to cancellation, correlation peaks can occur at the same time in the ++ and in the −+ frequency quadrants (*21*). Diagonal peaks are also present in the HYSCORE spectra due to the nonideality of the pulses generating an incomplete inversion of the magnetization by the π pulse (*15*).

Analysis of HYSCORE and ESEEM Spectra of H145A. In the HYSCORE spectra, nuclei close to cancellation can have peaks in both quadrants, the ++ and the −+ quadrants, albeit with different relative intensities. As a consequence, in the HYSCORE spectrum of H145A (Figure 4A), the ridges in the −+ quadrant have a higher resolution than those in the ++ quadrant. Therefore, the ridges in the −+ quadrant are used as the starting point of the analysis. The ridges a and b, which run parallel to the ν_2 frequency axis, reveal that 0.83 and 1.46 MHz correspond to NQ resonances originating from the α electron spin manifold (*22*, *23*). They are correlated to the frequency 4.19 MHz, i.e., $\nu_{dq\beta}$. This indicates that the frequencies 1.46, 0.83, and 4.19 MHz belong to the same nucleus, to which we will refer as N_a. In addition, the ridges d1, d, and e show that 1.54 and 0.80

Table 2: Quadrupole and Hyperfine Parameters of the Remote Nitrogens of the Coordinated Histidines (N_a, N_b) and of N of NO_2^- from HYSCORE and ESEEM Results

enzyme		e^2qQ/h[a] (MHz)	η	$\lvert A_{iso}\rvert$ (MHz)	$\lvert T\rvert$ (MHz)
H145A	N_a	−1.53	0.76	1.88	
	N_b	−1.56	0.90	1.57	
H145A (NO_2^-)	N_a	−1.53[b]	0.76[b]	1.69[c]	
	N_b	−1.56[b]	0.90[b]	1.41	
	$^{15}N(NO_2^-)$			0.50	0.90
	$^{14}N(NO_2^-)$	5.66[d]	0.31[d]	0.36	0.64

[a] Negative sign according to ref *37*. [b] Quadrupole values of N_a and N_b used in the simulation for H145A (NO_2^-) and obtained for N_a and N_b in H145A. [c] A_{iso} value calculated according to the shift observed for N_b (see text). [d] Quadrupole parameters of the ^{14}N nucleus of nitrite in a model compound (*26*) and used in the simulations of the ESEEM spectra. The hyperfine parameters for $^{14}N(NO_2^-)$ were calculated from those of $^{15}N(NO_2^-)$ taking into account the different nuclear g values.

MHz are NQ resonances that are correlated to $\nu_{dq\beta} = 3.87$ MHz. Thus, the frequencies 0.80, 1.54, and 3.87 MHz belong to a second nucleus, to which we will refer as N_b.

The correlations show that the bands in the ESEEM spectra of H145A at (0.59, 0.84, 1.44) MHz (high field, Figure 3C), at (0.58, 0.84, 1.47) MHz (intermediate field, Figure 3B), and at (0.61, 0.82, 1.46) MHz (low field, Figure 3A) derive from nucleus N_a and represent the NQ frequencies (ν_0, ν_-, ν_+) of N_a. From these frequencies the quadrupole parameters $|e^2qQ/h| = 1.53$ MHz and $\eta = 0.76$ are obtained. These NQ lines are correlated with $\nu_{dq\beta} = 4.19$ MHz. This results in $|A_{iso}|$ of 1.88 MHz (eq 4) for N_a (cf. Table 2).

The HYSCORE features corresponding to N_b indicate that the frequencies 0.80 and 1.54 MHz represent ν_- and ν_+ of N_b. This suggests that for this nucleus $\nu_0 = 0.74$ MHz, and bands around 0.7 MHz are indeed visible in the ESEEM spectra. From the NQ frequencies of this nucleus, the quadrupole parameters $|e^2qQ/h| = 1.56$ MHz and $\eta = 0.90$ are obtained. The HYSCORE spectrum shows that N_b has $\nu_{dq\beta} = 3.87$ MHz, revealing an $|A_{iso}|$ of 1.57 MHz (cf. Table 2).

Analysis of HYSCORE and ESEEM Spectra of H145A (NO_2^-). As the frequencies of the HYSCORE ridges and ESEEM bands associated with the single-quantum transitions do not change significantly upon binding nitrite, we conclude that the NQ frequencies of the nitrogens are conserved. The frequencies of the bands corresponding to the double-quantum transitions decrease in the ESEEM and HYSCORE spectra, showing that the isotropic hyperfine couplings of the nuclei decrease (cf. Table 2). Due to the reduction of the isotropic hyperfine coupling and to the increased width of the NQ lines, the HYSCORE ridges of N_a and N_b cannot be distinguished anymore. We therefore assume that A_{iso} of N_a and N_b is reduced by the same amount upon binding of NO_2^- to the site. The reduced intensity of the NQ bands in the ESEEM spectra can be a consequence of either the smaller hyperfine couplings or a variation in the relative orientation between the principal axes of the g-tensor and the quadrupole tensor of the respective nitrogens (*20*).

Signal of Nitrite Bound to H145A. The HYSCORE signal of the ^{15}N ($I = {}^1/_2$) nucleus of H145A ($^{15}NO_2^-$) appears in the ++ quadrant of the 2D spectrum (see Figure 4C, f), indicating that $A_{zz}(^{15}N) < 2\nu_I$ (*24*) and that the ridges are centered at (ν_I, ν_I). At $B_0 = 0.33$ T, ν_I of ^{15}N equals 1.42 MHz, the value at which the ridge intersects the diagonal. For a nuclear spin $I = {}^1/_2$, two transitions between the nuclear sublevels are expected, one for each electron spin manifold, ν_α and ν_β. The HYSCORE spectrum of a powder of such a spin system has ridges running approximately perpendicular to the frequency diagonal (*24*). For H145A ($^{15}NO_2^-$), the extent of the ridges shows the anisotropy of the nitrogen hyperfine coupling of $^{15}NO_2^-$. From the extension of these ridges, measured parallel to either one of the two frequency axes of the 2D spectrum, an estimate of the hyperfine parameters can be obtained (*24*). Assuming an equal sign of A_{iso} and T, an isotropic hyperfine coupling $|A_{iso}|$ of 0.50 ± 0.2 MHz and an anisotropy parameter $|T|$ of 0.90 ± 0.2 MHz results. The simulation of the HYSCORE signal using these hyperfine parameters is shown in Figure 5. Since the hyperfine parameters have been derived from the HYSCORE spectrum acquired at one value of B_0, the full anisotropic hyperfine tensor (*25*) has not been obtained. The point-dipole approximation cannot be applied for the analysis because of the small distance between the copper and the nitrogen of nitrite (2.48 Å).

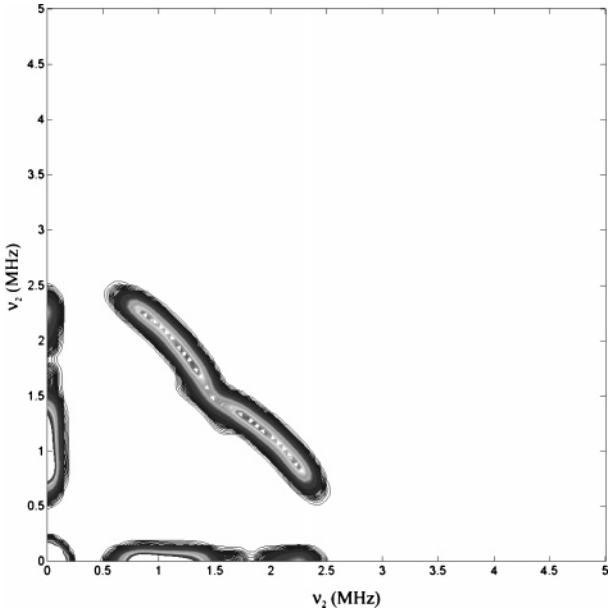

FIGURE 5: Simulation of the HYSCORE contour plot corresponding to the ^{15}N nucleus of nitrite in the type 2 copper site (see text).

Simulations of the ESEEM Spectra. Simulations of the ESEEM spectra of H145A (NO_2^-) are performed to determine the relative contribution to the spectra of the N_a and N_b nitrogens versus the NO_2^- nitrogen, in particular to understand why the NO_2^- nitrogen signal seems to contribute so little to the ESE modulations. Figures 6 and 7 show the result of such simulations. The middle traces in Figure 6 show the simulated contribution to the ESEEM spectra of the N_a and N_b nitrogens. The parameters used for the simulations are those reported in Table 2. For N_a and N_b the quadrupole values were used as determined for the unbound form of H145A. For the hyperfine tensors of these nitrogens only isotropic contributions were considered. The orientations of the quadrupole tensors are not meaningful, since their relative orientation with respect to the g-tensor is not known. To simulate the ESEEM spectra of the nitrogen of $^{14}NO_2^-$ bound to H145A, the quadrupole parameters for the nitrite nitrogen were taken as determined from an ESEEM study

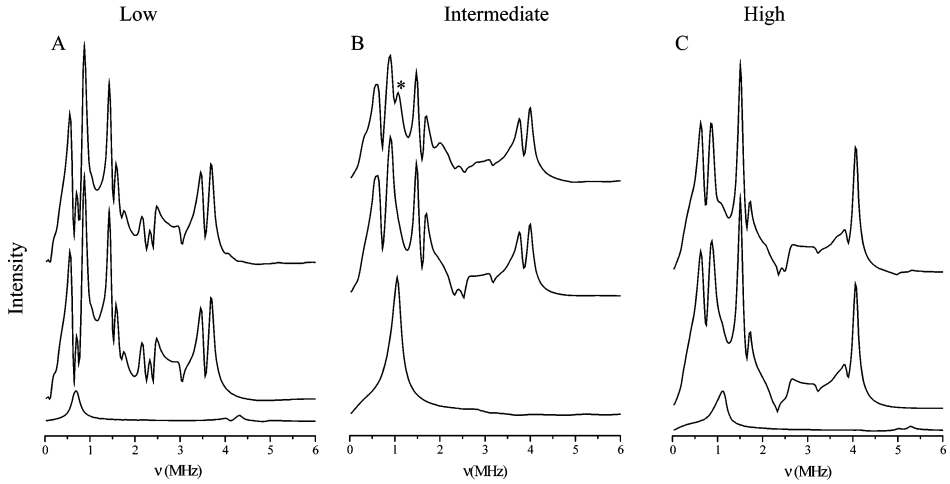

FIGURE 6: Simulations related to the ESEEM spectra of H145A ($^{14}NO_2^-$) at low (A), intermediate (B), and high (C) magnetic field values for a τ value of 140 ns. Each panel shows the simulated ESEEM spectrum corresponding to the contribution of the ^{14}N nucleus of nitrite (lower trace), the simulated ESEEM spectrum corresponding to the contributions of N_a and N_b (middle trace), and the simulated ESEEM spectrum corresponding to the contributions of N_a, N_b, and the ^{14}N of nitrite (upper trace).

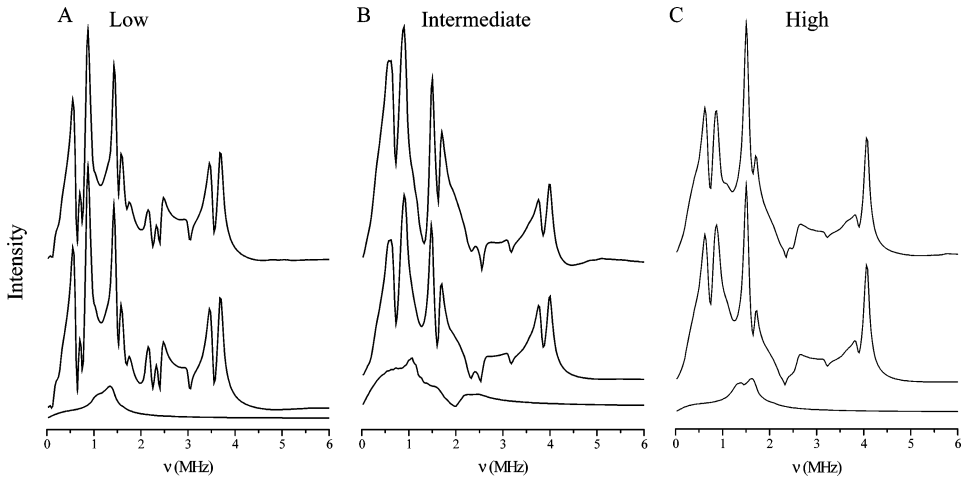

FIGURE 7: Simulations related to the ESEEM spectra of H145A ($^{15}NO_2^-$) at low (A), intermediate (B), and high (C) magnetic field values for a τ value of 140 ns. Each panel shows the simulated ESEEM spectrum corresponding to the contribution of the ^{15}N nucleus of nitrite (lower trace), the simulated ESEEM spectrum corresponding to the contributions of N_a and N_b (middle trace), and the simulated ESEEM spectrum corresponding to the contributions of N_a, N_b, and the ^{15}N of nitrite (upper trace).

of a model compound ($e^2qQ/h = 5.66$ MHz and $\eta = 0.31$) (*26*). The NQ frequencies (ν_0, ν_-, ν_+) corresponding to these quadrupole parameters are 0.9, 3.8, and 4.7 MHz, respectively, and in Figure 6, lower traces, the result of the simulation is shown. Except for the intermediate orientation, the intensity of the bands for the $^{14}NO_2^-$ nucleus is smaller than for N_a and N_b. The upper traces of Figure 6 show the result of simulations including three nuclei (N_a, N_b, and N of NO_2^-), to be compared with the experimental ESEEM spectra of Figure 3. The bands of the experimental ESEEM spectra are generally broader than the simulated ones, especially the double-quantum transitions around 3.5 MHz. These differences originate from the omission in the simulations of the anisotropic part of the hyperfine interaction of the two remote nitrogens. The relative intensities of the bands at the NQ frequencies, which depend strongly on the anisotropic hyperfine tensors and the orientation of the quadrupole principal axes (*20*), are also not reproduced.

The simulations confirm that the modulation originating from the nitrogen in nitrite has generally lower intensities with respect to that of N_a and N_b. The orientations of the principal axes of the quadrupole and hyperfine tensors used in the simulations shown in Figure 6 are chosen such as to reproduce the marked feature in the experimental ESEEM spectrum of H145A with $^{14}NO_2^-$ bound (Figure 3, intermediate field). The frequency of this feature coincides approximately with ν_0 of $^{14}NO_2^-$ and can thus be attributed to $^{14}NO_2^-$. Indeed, this band is absent in the ESEEM spectrum of H145A with $^{15}NO_2^-$ bound. For comparison, the simulations of H145A with $^{15}NO_2^-$ bound are reported in Figure 7. These simulations show that the ^{15}N of $^{15}NO_2^-$ produces a change in the amplitude and line width of the ESEEM bands (mainly at intermediate field), but there are no intense, narrow bands to be expected for this nucleus. The simulation of the ESEEM and HYSCORE spectra confirms that, although the ESEEM signal of the nitrite nitrogen is quite weak and not clearly distinguishable from the other contributions, it is revealed by HYSCORE experiments. The increased spectral resolution of the two-dimensional experiment allowed a resolution of the nitrogen signal of nitrite.

DISCUSSION

The electronic structure of the substrate bound to the active site of NiR is investigated by HYSCORE and ESEEM

spectroscopy on the resting state of the enzyme and the substrate-bound form. Experiments were performed on the H145A mutant, in which the absence of the type 1 copper signal (*14*) allows to selectively investigate the type 2 copper site. This enabled to perform ESEEM and HYSCORE experiments along the three principal directions of the *g*-tensor of the type 2 copper site, which are not accessible using wild-type NiR. The cw EPR spectra of H145A and H145A (NO_2^-) (Figure 2) show the full conversion of the type 2 site to the nitrite-bound form, unambiguously proving that the ESEEM and HYSCORE results derive from a single species.

The X-band ESEEM and HYSCORE experiments on frozen solutions of H145A yield hyperfine and quadrupole parameters of two nitrogens of the type 2 copper of the enzyme and reveal the changes of these values induced by nitrite binding ($^{14}NO_2^-$) (Table 2). By isotopic substitution ($^{15}NO_2^-$), the spectral signatures of the substrate nitrogen are unambiguously identified. The HYSCORE experiments displayed a signal of $^{15}NO_2^-$ bound to H145A, from which hyperfine parameters of the nitrite nitrogen were estimated. We will discuss the results obtained and compare them with those from related investigations in the literature.

The cw EPR Spectra. Simulation of the X-band cw EPR spectra of NiR and its mutant H145A with and without nitrite bound yields the copper EPR parameters of the different enzymes and their change upon nitrite binding (Table 1). The cw EPR spectra at X-band reveal a slight increase of g_{zz} and a decrease of the A_{zz} values of the type 2 copper site of H145A with respect to NiR. Notably, these changes in the type 2 copper site are induced by a change in the first coordination of the type 1 copper site, 12.5 Å away from the type 2 site. Similar observations were previously reported (*4*) for another mutant of NiR, in which the methionine axial ligand of the type 1 copper was replaced by a glutamate.

The EPR parameters of the H145A mutant, although not identical to those of the wt NiR, are close enough to consider the type 2 site of this mutant a proper model to study the binding of NO_2^- in NiR. As Table 1 shows, the changes of the g values and of A_{zz} going from wt NiR to H145A are minor compared to the changes upon NO_2^- binding. This binding reduces g_{zz} by as much as 0.053, results in a large rhombicity ($g_{yy} - g_{xx} = 0.085$), and reduces the value of A_{zz} to 118×10^{-4} cm^{-1}. This brings A_{zz} out of the range commonly observed for type 2 copper sites ($\geq 140 \times 10^{-4}$ cm^{-1}) (*27*). Also, the significant rhombicity is not compatible with the close to axial *g*-tensor characteristic of most type 2 sites (cf. $g_{yy} - g_{xx} = 0$ and 0.007 for the type 2 site of wt NiR and H145A, respectively). For type 1 copper sites the rhombicity is usually bigger, as the present case of NiR (0.030) reveals as well. It is interesting to compare the rhombicity of the *g*-tensor of H145A (NO_2^-) with that of azurin (*28*), which contains a typical type 1 copper site, and that of the M121Q mutant of azurin (*29*) with a copper site resembling that of stellacyanin (*30*). While the rhombicity amounts to 0.017 for azurin, it becomes 0.055 for the mutant in which the weakly bound axial ligand methionine is replaced by glutamine. The glutamine in M121Q provides for a strongly bound oxygen ligand, and the rhombicity derives from the d_z^2 character (*31*) mixed into the singly occupied molecular orbital, which has predominant copper d_{xy} character. Correspondingly, the large rhombicity for H145A (NO_2^-) might well indicate an axial binding of nitrite through the formation of a copper−nitrite bond involving the copper d_z^2 orbital. Both the value of A_{zz} and the rhombicity of the *g*-tensor indicate that the type 2 copper site of H145A adopts a more type 1-like character upon binding of NO_2^-.

Nitrogen Hyperfine and Quadrupole Parameters of the Type 2 Site. The two inequivalent nitrogens N_a and N_b in H145A are assigned to the remote nitrogens of two histidines on the basis of their quadrupole parameters. These parameters are similar to those of the protonated nitrogens of solid imidazole (*32*).

Previously, from ENDOR spectroscopy at Q-band on NiR, isotropic hyperfine couplings of 36.7 and 30.5 MHz for two copper-bound nitrogens of histidines were reported (*12*). Assuming that the ratio of A_{iso} of coordinated versus remote nitrogens in histidines is 20 (*33*), the values of the remote nitrogens N_a and N_b from the ESEEM experiments would correspond to A_{iso} values of 37.6 and 31.4 MHz for the coordinated nitrogens, in good agreement with the values of Veselov et al. (*12*). In our work, no indication of a hyperfine coupling of the third histidine of the site is found. Veselov et al. (*12*) assign a hyperfine coupling of 18.8 MHz to the coordinating nitrogen of the third histidine. The corresponding remote nitrogen in that case would have a hyperfine coupling too far from cancellation to produce signals that would be strong enough to be detected by ESEEM in the presence of the intense quadrupole transitions of the other nitrogens. Upon binding nitrite to the site, the A_{iso} values of N_a and N_b decrease by approximately 11%, in agreement to what is observed for the coordinating nitrogens in ref *12*. This reduction of A_{iso} is in the same range as the reduction of the copper A_{zz} upon nitrite binding (Table 1). The changes in the line width and intensity of the bands in the ESEEM spectra suggest that in addition to the reduction of A_{iso} there could also be a change of the relative orientation between the quadrupole tensor principal axes of these nitrogens and the *g*-tensor principal axes upon binding nitrite. This could be brought about by a small reorientation of the histidine rings upon binding of nitrite, as observed by X-ray crystallography (*5*) or a reorientation of the *g*-tensor principal axes of the copper site in the presence of nitrite.

The reduction of A_{iso} of the imidazole nitrogens reflects a reduction of the spin density on the ligands as had been suggested before (*12*). Since also the copper hyperfine coupling (A_{zz}) decreases, a straightforward shift of the spin density from the ligands toward copper seems unlikely. This finding and the changes in the *g*-tensor reveal a change in the composition of the SOMO upon nitrite binding.

The HYSCORE experiments revealed a signal from the nitrogen of $^{15}NO_2^-$ bound to H145A. Two reasons may have prevented the observation of the signal of the nitrite nitrogen in previous investigations. Veselov et al. (*12*) have recorded the ENDOR spectra at the low-field edge of the EPR spectrum (g_{zz}) in order to unequivocally interrogate the type 2 site of NiR. In the present study, the use of H145A allowed to acquire spectra at the intermediate- and high-field (g_{xx} and g_{yy}) region of the EPR spectrum without interference from signals of the type 1 copper. Moreover, the observed hyperfine coupling of the nitrite nitrogen of 0.3−0.9 MHz would result in ENDOR signals at frequencies too low to be detected in that experiment.

Binding Mode of Nitrite. The hyperfine coupling of the nitrogen of $^{15}NO_2^-$ bound to H145A, which had not previously been determined, reveals information on the binding mode of nitrite. The value of 0.36 MHz of A_{iso} for the nitrogen of $^{14}NO_2^-$ can be compared with that of 3.4 MHz for ^{14}N in nitrite equatorially coordinated in the model compound $[Cu^{2+}(TEPA)(NO_2)]PF_6$ (TEPA = tris[2-(2-pyridyl)ethyl]amine) (*26*). The A_{iso} value of the $^{14}NO_2^-$ bound to H145A is significantly smaller than that for the model compound, which indicates that the substrate is coordinated to the enzyme in a position approximately axial.

Also, another observation points toward an axial binding of the substrate. The A_{iso} of the three nitrogens directly coordinated to copper in the type 2 site of NiR are all larger than 18 MHz (*12*). This would suggest that all of the three imidazole nitrogens directly coordinated to copper in the type 2 site of NiR are in the equatorial plane. Thus, only the axial position is available for the coordination of the substrate. An axial coordination by a nitrogen atom of a ligand, as observed for pyridine coordinated to Cu^{2+}(benzoylacetonate), resulted in an A_{iso} of the nitrogen of 0.7 MHz (*34*).

The value of the isotropic hyperfine coupling constant of the nitrogen in $^{14}NO_2^-$ bound to H145A compared to that of the model compound (*26*) shows that there is a small but not negligible delocalization of the unpaired electron onto the substrate in H145A. This is another indication that substrate binding induces a change of the composition of the SOMO, which enables overlap with an orbital of the axially bound substrate. The hyperfine coupling observed for the nitrite and the reduction of spin density on the remaining ligands and on copper, together with the changes in the copper *g*-tensor parameters, further suggest a rearrangement of the copper d orbitals upon substrate binding.

Implications for the Mechanism of Nitrite Reduction. The electronic structure of the site changes upon substrate binding. These changes involve the following: (i) the admixture of the d_z^2 orbital, which provides overlap with the substrate since it is oriented toward the axially bound nitrite. Concomitantly, (ii) a redistribution of the SOMO over the ligands takes place. The hyperfine couplings of the coordinated histidines and the copper hyperfine coupling A_{zz} decrease upon substrate binding. The isotropic hyperfine coupling of the nitrite nitrogen reveals that the SOMO extends onto the nitrite. Thus, apparently, spin density from the other ligands is transferred to the nitrite. As the SOMO is the accepting orbital for the electron that reduces the type 2 copper site and ultimately the nitrite, delocalization onto the nitrite is needed for the reaction to occur.

For the reaction to proceed, one N−O bond of the nitrite has to be broken. Antibonding character of the SOMO with respect to the N−O bond would promote the reaction, because electron transfer into this orbital would weaken the N−O bond and could thus trigger the reaction. According to crystallographic evidence (*6*, *35*), the nitrite is bound "face on" with respect to the copper; i.e., the O−N−O plane is tilted by 75° relative to the Cu−O−O plane. This enables the overlap of the d_z^2 orbital on copper with the π electron system of the nitrite, suggesting that the SOMO on the nitrite has π electron character, similar to the frontier orbitals (the HOMO and the LUMO) of the isolated nitrite. This indicates that an antibonding character of the SOMO with respect to the N−O bond is indeed probable, given that the HOMO and the LUMO of the isolated nitrite have such an antibonding character. To experimentally verify the character of the SOMO on the nitrite, hyperfine information from the other nuclei of nitrite would be needed.

The results of the present study reveal that the SOMO of the substrate-bound enzyme extends over the nitrite and suggest changes in electronic structure induced by nitrite binding that most probably promote the enzymatic reaction of NiR. Several questions remain to be answered: It stands to reason that the rehybridization at copper also brings about a change in redox potential (*36*) and affects the rate of electron transfer from the type 1 to the type 2 site after nitrite binding at certain pH values (*8*, *36*). An indication seems to be that the EPR parameters of the site change in the direction toward the parameters of the type 1 site and that, in general, type 1 sites are more easily reduced than type 2 sites. To prove this, a full analysis of the electronic structure of the type 2 site would be needed. Experiments in progress to determine the *g*-tensor anisotropy of the type 2 site in the substrate-bound form will be the basis of such an analysis.

ACKNOWLEDGMENT

We gratefully acknowledge Maurice van Gastel for kind assistance during the simulations of ESEEM and HYSCORE spectra and Karen Vastenhoud for participation in the measurements.

REFERENCES

1. Suzuki, S., Kataoka, K., Yamaguchi, K., Inoue, T., and Kai, Y. (1999) Structure−Function Relationships of Copper-Containing Nitrite Reductases, *Coord. Chem. Rev. 192*, 245−265.
2. Murphy, M. E. P., Turley, S., Kukimoto, M., Nishiyama, M., Horinouchi, S., Sasaki, H., Tanokura, M., and Adman, E. T. (1995) Structure of *Alcaligenes faecalis* Nitrite Reductase and a Copper Site Mutant, M150E, that Contains Zinc, *Biochemistry 34*, 12107−12117.
3. Dodd, F. E., Van Beeumen, J., Eady, R. R., and Hasnain, S. S. (1998) X-ray Structure of a Blue-Copper Nitrite Reductase in Two Crystal Forms. The Nature of the Copper Sites, Mode of Substrate Binding and Recognition by Redox Partner, *J. Mol. Biol. 282*, 369−382.
4. Kukimoto, M., Nishiyama, M., Murphy, M. E. P., Turley, S., Adman, E. T., Horinouchi, S., and Beppu, T. (1994) X-ray Structure and Site-Directed Mutagenesis of a Nitrite Reductase from *Alcaligenes faecalis* S-6—Roles of 2 Copper Atoms in Nitrite Reduction, *Biochemistry 33*, 5246−5252.
5. Murphy, M. E. P., Turley, S., and Adman, E. T. (1997) Structure of Nitrite Bound to Copper-Containing Nitrite Reductase from *Alcaligenes faecalis*—Mechanistic Implications, *J. Biol. Chem. 272*, 28455−28460.
6. Tocheva, E. I., Rosell, F. I., Mauk, A. G., and Murphy, M. E. P. (2004) Side-On Copper-Nitrosyl Coordination by Nitrite Reductase, *Science 304*, 867−870.
7. Suzuki, S., Furusawa, H., Kataoka, K., Yamaguchi, K., Kobayashi, K., and Tagawa, S. (2000) Intramolecular Electron-Transfer Process of Native and Mutant Forms of Blue Copper-Containing Nitrite Reductase from *Alcaligenes xylosoxidans*, *Inorg. React. Mech. 2*, 129−135.
8. Suzuki, S., Kataoka, K., and Yamaguchi, K. (2000) Metal Coordination and Mechanism of Multicopper Nitrite Reductase, *Acc. Chem. Res. 33*, 728−735.
9. Suzuki, S., Kohzuma, T., Deligeer, Yamaguchi, K., Nakamura, N., Shidara, S., Kobayashi, K., and Tagawa, S. (1994) Pulse-Radiolysis Studies on Nitrite Reductase from Achromobacter Cycloclastes Iam-1013—Evidence for Intramolecular Electron-Transfer from Type-1 Cu to Type-2 Cu, *J. Am. Chem. Soc. 116*, 11145−11146.
10. Prudencio, M., Eady, R. R., and Sawers, G. (2001) Catalytic and Spectroscopic Analysis of Blue Copper-Containing Nitrite Re-

ductase Mutants Altered in the Environment of the Type 2 Copper Centre: Implications for Substrate Interaction, *Biochem. J. 353*, 259−266.
11. Howes, B. D., Abraham, Z. H. L., Lowe, D. J., Bruser, T., Eady, R. R., and Smith, B. E. (1994) EPR and Electron-Nuclear Double-Resonance (ENDOR) Studies Show Nitrite Binding to the Type-2 Copper Centers of the Dissimilatory Nitrite Reductase of *Alcaligenes xylosoxidans* (Ncimb-11015), *Biochemistry 33*, 3171−3177.
12. Veselov, A., Olesen, K., Sienkiewicz, A., Shapleigh, J. P., and Scholes, C. P. (1998) Electronic Structural Information from Q-band ENDOR on the Type 1 and Type 2 Copper Liganding Environment in Wild-Type and Mutant Forms of Copper-Containing Nitrite Reductase, *Biochemistry 37*, 6095−6105.
13. Zhao, Y. W., Lukoyanov, D. A., Toropov, Y. V., Wu, K., Shapleigh, J. P., and Scholes, C. P. (2002) Catalytic Function and Local Proton Structure at the Type 2 Copper of Nitrite Reductase: The Correlation of Enzymatic pH Dependence, Conserved Residues, and Proton Hyperfine Structure, *Biochemistry 41*, 7464−7474.
14. Wijma, H. J., Boulanger, M. J., Molon, A., Fittipaldi, M., Huber, M., Murphy, M. E. P., Verbeet, M. P., and Canters, G. W. (2003) Reconstitution of the Type-1 Active Site of the H145G/A Variants of Nitrite Reductase by Ligand Insertion, *Biochemistry 42*, 4075−4083.
15. Schweiger, A., and Jeschke, G. (2001) *Principles of Pulse Electron Paramagnetic Resonance*, Oxford University Press, Oxford.
16. van Gastel, M., Coremans, J. W. A., Jeuken, L. J. C., Canters, G. W., and Groenen, E. J. J. (1998) Electron-Spin-Echo Envelope Modulation Spectrum of Azurin at X-band, *J. Phys. Chem. A 102*, 4462−4470.
17. Brecht, M., van Gastel, M., Buhrke, T., Friedrich, B., and Lubitz, W. (2003) Direct Detection of a Hydrogen Ligand in the [NiFe] Center of the Regulatory H2-Sensing Hydrogenase from *Ralstonia eutropha* in its Reduced State by HYSCORE and ENDOR Spectroscopy, *J. Am. Chem. Soc. 125*, 13075−13083.
18. Dikanov, S. A., and Tsvetkov, Y. D. (1992) *Electron Spin-Echo Envelope Modulation (ESEEM) Spectroscopy*, CRC Press, Boca Raton, FL.
19. Mims, W. B., and Peisach, J. (1978) Nuclear Modulation Effect in Electron-Spin-Echoes for Complexes of Cu^{2+} and Imidazole with ^{14}N and ^{15}N, *J. Chem. Phys. 69*, 4921−4930.
20. Flanagan, H. L., and Singel, D. J. (1987) Analysis of ^{14}N ESEEM Patterns of Randomly Oriented Solids, *J. Chem. Phys. 87*, 5606−5616.
21. Shane, J. J., Höfer, P., Reijerse, E. J., and de Boer, E. (1992) Hyperfine Sublevel Correlation Spectroscopy (HYSCORE) of Disordered Solids, *J. Magn. Reson. 99*, 596−604.
22. Tyryshkin, A. M., Dikanov, S. A., Reijerse, E. J., Burgard, C., and Hüttermann, J. (1999) Characterization of Bimodal Coordination Structure in Nitrosyl Heme Complexes through Hyperfine Couplings with Pyrrole and Protein Nitrogens, *J. Am. Chem. Soc. 121*, 3396−3406.
23. Harmer, J., Van Doorslaer, S., Gromov, I., and Schweiger, A. (2002) Corrin Nitrogens and Remote Dimethylbenzimidazole Nitrogen Interactions in Cob(II)alamin Studied with HYSCORE at X- and Q-band, *Chem. Phys. Lett. 358*, 8−16.
24. Höfer, P. (1994) Distortion-Free Electron-Spin-Echo Envelope-Modulation Spectra of Disordered Solids Obtained from 2-Dimensional and 3-Dimensional HYSCORE Experiments, *J. Magn. Reson., Ser. A 111*, 77−86.
25. Dikanov, S. A., and Bowman, M. K. (1995) Cross-Peak Lineshape of 2-Dimensional ESEEM Spectra in Disordered S = 1/2, I = 1/2 Spin Systems, *J. Magn. Reson., Ser. A 116*, 125−128.
26. Jiang, F., Conry, R. R., Bubacco, L., Tyeklar, Z., Jacobson, R. R., Karlin, K. D., and Peisach, J. (1993) Crystal-Structure and Electron-Spin-Echo Envelope Modulation Study of [Cu(II)(Tepa)-(NO2)]Pf6 (Tepa = Tris[2-(2-pyridyl)ethyl]amine)—A Model for the Purported Structure of the Nitrite Derivative of Hemocyanin, *J. Am. Chem. Soc. 115*, 2093−2102.
27. Peisach, J., and Blumberg, W. E. (1974) Structural Implications Derived from Analysis of Electron-Paramagnetic Resonance-Spectra of Natural and Artificial Copper Proteins, *Arch. Biochem. Biophys. 165*, 691−708.
28. Coremans, J. A., Poluektov, O. G., Groenen, E. J., Canters, G. W., Nar, H., and Messerschmidt, A. (1994) A W-Band Electron-Paramagnetic-Resonance Study of a Single Crystal of Azurin, *J. Am. Chem. Soc. 116*, 3097−3101.
29. Coremans, J. A., Poluektov, O. G., Groenen, E. J., Warmerdam, G. M., Canters, G. W., Nar, H., and Messerschmidt, A. (1996) The Azurin Mutant Met121Gln: A Blue-Copper Protein with a Strong Axial Ligand, *J. Phys. Chem. 100*, 19706−19713.
30. Malmström, B. G., Reinhamm, B., and Vänngård, T. (1970) State of Copper in Stellacyanin and Laccase from Lacquer Tree *Rhus vernicifera*, *Biochim. Biophys. Acta 205*, 48−57.
31. Gewirth, A. A., Cohen, S. L., Schugar, H. J., and Solomon, E. I. (1987) Spectroscopic and Theoretical-Studies of the Unusual Electron-Paramagnetic-Resonance Parameters of Distorted Tetrahedral Cupric Sites—Correlations to X-ray Spectral Features of Core Levels, *Inorg. Chem. 26*, 1133−1146.
32. Hunt, M. J., Mackay, A. L., and Edmonds, D. T. (1975) Nuclear Quadrupole Resonance of ^{14}N in Imidazole and Related Compounds, *Chem. Phys. Lett. 34*, 473−475.
33. Coremans, J. W. A., Poluektov, O. G., Groenen, E. J. J., Canters, G. W., Nar, H., and Messerschmidt, A. (1996) A W-band Electron Nuclear Double Resonance Study of Single Crystals of ^{14}N and ^{15}N Azurin, *J. Am. Chem. Soc. 118*, 12141−12153.
34. Cornelius, J. B., McCracken, J., Clarkson, R. B., Belford, R. L., and Peisach, J. (1990) Electron-Spin-Echo Envelope Modulation Angle Selection Studies of Axial Pyridine Coordination to Copper-(II) Benzoylacetonate, *J. Phys. Chem. 94*, 6977−6982.
35. Adman, E. T., Godden, J. W., and Turley, S. (1995) The Structure of Copper-Nitrite Reductase from *Achromobacter cycloclastes* at 5 pH Values, with NO_2^- Bound and with Type-II Copper Depleted, *J. Biol. Chem. 270*, 27458−27474.
36. Kobayashi, K., Tagawa, S., Deligeer, and Suzuki, S. (1999) The pH-Dependent Changes of Intramolecular Electron Transfer on Copper-Containing Nitrite Reductase, *J. Biochem. 126*, 408−412.
37. Palmer, M. H., Scott, F. E., and Smith, J. A. S. (1983) Calculation of the ^{14}N and ^{2}H Quadrupole Coupling Tensor in Trimeric Imidazole, *Chem. Phys. 74*, 9−14.

BI0513913